Numerical calculations are easily accomplished with a computer.

ACKNOWLEDGMENT

The author wishes to thank Dr. Leo Young, Dr. E. G. Cristal, L. Robinson, and B. M. Schiffman for helpful discussions and useful suggestions.

REFERENCES

[1] J. J. Bolljahn and G. L. Matthaei, "A study of the phase and filter properties of arrays of parallel conductors between ground planes," *Proc. IRE*, vol. 50, Mar. 1962, pp. 299–311.
[2] H. S. Hewitt, "A computer designed, 720 to 1 microwave compression filter," *IEEE Trans. Microwave Theory Tech.*, vol. MTT-15, Dec. 1967, pp. 687–694.
[3] Kuroda, "Derivation methods of distributed constant filters from lumped constant filters" (in Japanese), Lectures at Joint Meetings of Kansai Branch of Three Institutes, Japan, 1952.
[4] R. Levy, "A general equivalent circuit transformation for distributed networks," *IEEE Trans. Circuit Theory* (Corresp.), vol. CT-12, Sept. 1965, pp. 457–458.
[5] K. K. Pang, "A new transformation for microwave network synthesis," *IEEE Trans. Circuit Theory* (Corresp.), June 1966, pp. 235–238.
[6] R. Sato, "A design method for meander-line networks using equivalent circuit transformations," in *1969 IEEE Symp. Circuit Theory Dig.*, pp. 70–71.
[7] R. Sato, "Two universal transformations for commensurate distributed circuits," *Electron. Lett.*, to be published.
[8] R. Sato and E. G. Cristal, "Simplified analysis of coupled transmission-line networks" *IEEE Trans. Microwave Theory Tech.*, vol. MTT-18, Mar. 1970, pp. 122–131.
[9] P. I. Richards, "Resistor-transmission-line circuits," *Proc. IRE*, vol. 36, Feb. 1948 pp. 217–220.
[10] R. Sato, *Transmission Circuits* (Denso-Kairo), in Japanese. Tokyo, Japan: Korona-sha Publ. Co., 1963.
[11] H. Uchida, *Fundamentals of Coupled Lines and Multi-Wire Antennas*. Sendai, Japan: Sasaki Publ. Co., 1967.

Reciprocal and Nonreciprocal Modes of Propagation in Ferrite Stripline and Microstrip Devices

MARION E. HINES, FELLOW, IEEE

Abstract—**An approximate analysis is presented together with a physical description of the modes of propagation in stripline and microstrip devices of significant width, using ferrite slabs as dielectric material, magnetized perpendicular to the ground plane. The dominant mode resembles TEM propagation, except that there is a strong transverse field displacement, causing wave energy to be concentrated along one edge of the line. Nonreciprocal behavior is obtainable by asymmetrically loading the edges. Approximate analytical techniques are given for isolators and phase shifters, with examples of numerical computations and experimental results.**

I. INTRODUCTION

SOME of the modes of propagation in strip-line and microstrip transmission lines using ferrite slabs as dielectric material are described. A new form of isolator and a new nonreciprocal phase shifter are also described which utilize these transmission media. In all cases magnetization is perpendicular to the ground plane. Approximate analytic treatments are presented, based upon solutions of Maxwell's equations in alternative geometrical models, intuitively deduced to be qualitatively equivalent. Exact treatments of the boundary problems appear to be intractable.

Manuscript received July 21, 1970; revised November 9, 1970. This work was supported in part by the U. S. Army Advanced Ballistic Missile Defense Agency under Contract DAAB07-69-C-0445.
The author is with Microwave Associates, Inc., Burlington, Mass. 01803.

These new devices have several desirable properties and are adaptable for use in microwave integrated circuitry. Use of the isolator in a distributed negative-resistance diode amplifier has already been described [1]. Because of certain unique properties of the transmission modes, still other applications may be found in the future. The work reported here was undertaken to provide quantitative approximations for the propagation constants and the field configurations of the various modes and to provide a design theory for practical nonreciprocal devices in these configurations.

Figs. 1 and 2 illustrate these configurations. It is assumed that the center (or upper) conductor is substantially wide compared with the thickness of the ferrite, with most of the RF energy in the rectangular zone I between the conductors. The fringing-field zones II and III at the edges are treated as special boundaries which modify the propagation characteristics.

TM modes are normally impossible between parallel plates when the spacing is less than one half-wavelength and are not, therefore, included in this analysis. In zone I simple TE modes are assumed, with field components E_z, H_x, and H_y. E_z is assumed to be invariant with z. Only the ordinary macroscopic waves are considered at frequencies well removed from the resonance frequency γH_i. Some of the most interesting cases are

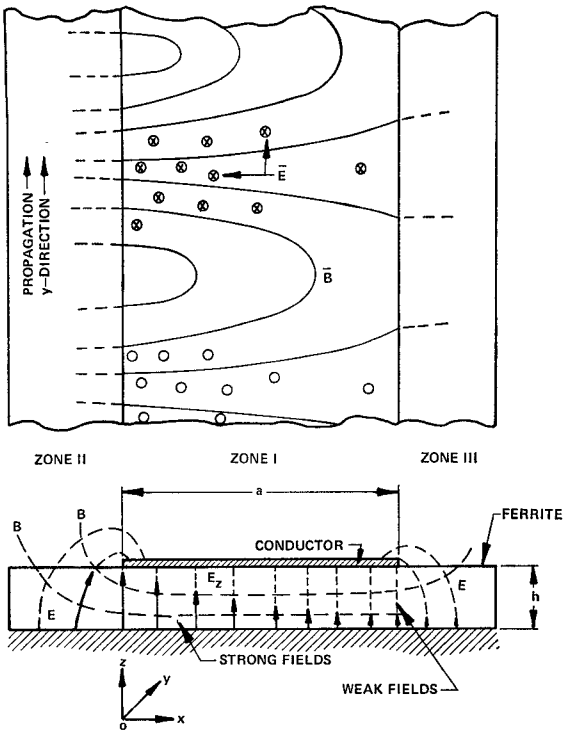

Fig. 1. Microstrip line showing RF fields of dominant mode. Dc magnetization is in z direction.

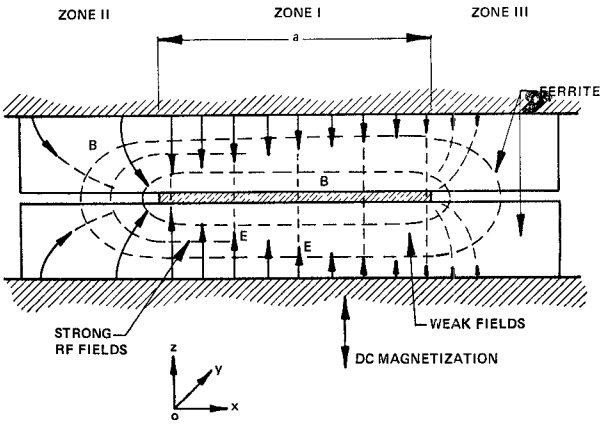

Fig. 2. Cross section of stripline showing RF fields of dominant mode.

computed for the condition of a highly magnetized (commonly, but not necessarily, saturated) material with a low internal field H_i, often assumed to be zero.

Figs. 1 and 2 show sketches of the RF fields $\overline{E}$ and $\overline{B}$ for the dominant mode of propagation. It is seen that there is a strong variation of field quantities transverse to the direction of propagation. The RF energy tends to be concentrated at one side in lines of significant width. This "field displacement" effect is reversed for the two opposite directions of wave propagation. It will also be reversed by reversing the direction of the magnetization. This effect is used to provide the nonreciprocal behavior of the new isolator and phase shifter devices which are described.

II. Basic Equations

The analytical approach is to divide the device into three longitudinal zones as shown in Figs. 1 and 2. Zone I is the central region between the upper (or central) conductor and the ground plane (or planes), which we analyze in rectangular coordinates. Zones II and III are fringing-field zones which may contain other intentional perturbations. These edge zones form the boundaries for zone I. General solutions to Maxwell's equations are written for zone I, and the propagation constants are determined by matching the boundary admittances of zones II and III at $x=0$ and at $x=a$. Various approximations for the edge admittances are used in specific cases in following sections.

Assuming only the field quantities E_z, H_y, and H_x, TE solutions for Maxwell's equations can be found in various standard texts [2], [3]. Treatment of zone I is identical for the two geometries. In the stripline case, time-phase is reversed in the upper half and all field quantities are as mirror images in the two halves. In these equations, MKS formulations are used with $\mu_0=4\pi\times10^{-7}$ H/m and $\epsilon_0=1/36\pi\times10^{-9}$ F/m. The quantities ϵ_f, μ, and K are dimensionless relative quantities relating to the ferrite material. Using A and B as arbitrary constants, γ_x and γ_y as propagation constants, and $e^{j\omega t}$ understood, the field equations are written directly:

$$E_z = \left\{Ae^{-\gamma_x x} + Be^{+\gamma_x x}\right\}e^{-\gamma_y y} \tag{1}$$

$$H_y = \frac{1}{\omega\mu_0\mu_{eq}}\left\{A\left(j\gamma_x - \frac{K}{\mu}\gamma_y\right)e^{-\gamma_x x} + B\left(-j\gamma_x - \frac{K}{\mu}\gamma_y\right)e^{+\gamma_x x}\right\}e^{-\gamma_y y} \tag{2}$$

$$H_x = \frac{1}{\omega\mu_0\mu_{eq}}\left\{A\left(-\frac{K}{\mu}\gamma_x - j\gamma_y\right)e^{-\gamma_x x} + B\left(\frac{K}{\mu}\gamma_x - j\gamma_y\right)e^{+\gamma_x x}\right\}e^{-\gamma_y y}. \tag{3}$$

The propagation constants are related by the equation

$$\gamma_x^2 + \gamma_y^2 + \omega^2\mu_0\epsilon_0\mu_{eq}\epsilon_f = 0. \tag{4}$$

In the preceding, μ and K are the diagonal and off-diagonal coefficients of the permeability tensor for magnetization in the z direction. For complete derivations the reader should consult the texts referenced. For the lossless case, assumed here, these are approximated:

$$\mu = 1 + \frac{\omega_0\omega_m}{\omega_0^2 - \omega^2} \tag{5}$$

$$K = \frac{\omega\omega_m}{\omega_0^2 - \omega^2}. \tag{6}$$

The equivalent permeability μ_{eq} is given by

$$\mu_{eq} = \frac{\mu^2 - K^2}{\mu}. \tag{7}$$

Also, ω_0 is the gyromagnetic resonance frequency proportional to the internal magnetic field H_i and ω_m is a magnetization frequency related to the induced magnetization of the ferrite,

$$\omega_0 = -\gamma H_i \tag{8}$$

$$\omega_m = -\gamma M. \tag{9}$$

(If H_i is in oersteds and $4\pi M$ is in gauss, then $\gamma/2\pi \simeq 2.8$ MHz/Oe.)

In the general field equations (1)–(3) γ_x and γ_y may be real, complex, or imaginary. For lossless propagation in the $+y$ direction, γ_y is positive imaginary, but, γ_x may be either purely real or purely imaginary, depending upon the boundary conditions and the mode involved. In the isolator solutions given later, both γ_x and γ_y are complex, where

$$\gamma_x = \alpha_x + j\beta_x \tag{10}$$

$$\gamma_y = \alpha_y + j\beta_y. \tag{11}$$

III. First Approximation: Neglect of Fringing Fields

For thin ferrite slabs with a significant width of conductor, only a small fraction of the RF energy will be involved in the fringing fields. Particularly in the stripline case with mirror symmetry about the central plane, there can be but little current in the center conductor directed transversely at the edge. This implies the boundary condition $H_y = 0$ at $x = 0$ and at $x = a$. (In the microstrip case, this is less accurate, but is believed to be qualitatively meaningful in many cases. In Section V we present a better estimate for the boundary cases.) The boundary condition $H_y = 0$ at $x = 0$ and $x = a$ is equivalent to a hypothetical magnetic wall at the planes $x = 0$ and $x = a$.

Case 1: Very Wide or Semi-Infinite Line

Here, solutions exist for a unidirectional wave confined to a single edge. For assumed lossless propagation with finite energy, we take

$$\begin{aligned} B &= 0 \\ \beta_x &= 0 \\ \alpha_y &= 0. \end{aligned} \tag{12}$$

The field equations can be simplified as follows:

$$E_z = Ae^{-\alpha_x x}e^{-j\beta_y y} \tag{13}$$

$$H_y = \frac{jA}{\omega\mu_0\mu_{eq}}\left\{\alpha_x - \frac{K}{\mu}\beta_y\right\}e^{-\alpha_x x}e^{-j\beta_y y} \tag{14}$$

$$H_x = \frac{A}{\omega\mu_0\mu_{eq}}\left\{-\frac{K}{\mu}\alpha_x + \beta_y\right\}e^{-\alpha_x x}e^{-j\beta_y y}. \tag{15}$$

For the boundary condition $H_y = 0$ at $x = 0$, we write, from (14),

$$\alpha_x - \frac{K}{\mu}\beta_y = 0 \tag{16}$$

which can be directly solved through the use of (4) to give

$$\beta_y = \omega\sqrt{\mu_0\epsilon_0\epsilon_f\mu} \tag{17}$$

$$\alpha_x = \omega\frac{K}{\mu}\sqrt{\mu_0\epsilon_0\epsilon_f\mu}. \tag{18}$$

This is the edge-guided mode.

The field patterns are similar to those of Figs. 1 and 2, assuming that the width a becomes very large and that the fields decay exponentially to negligible values at large x. Note that Figs. 1 and 2 show $\overline{B}$ lines, rather than $\overline{H}$. In Maxwell's equations, div $\overline{B} = 0$, and here, div $\overline{H} \neq 0$. The $\overline{H}$ lines are purely transverse and simply fade away with increasing x. $H_y = 0$ everywhere and this is a TEM mode in this approximation, but note that $B_y \neq 0$ because of the tensor relationship.

A characteristic impedance can be determined in three different formulations. For the wave impedance,

$$\frac{E_z}{H_x} = \sqrt{\frac{\mu_0\mu}{\epsilon_0\epsilon_f}} \text{ ohms per square.} \tag{19}$$

An alternative form relates the impedance to the power and the total y-directed current,

$$Z_{0I} = \frac{P}{I_y^2} = \frac{\omega\mu_0 hK}{2} \text{ ohms.} \tag{20}$$

In terms of the voltage at the edge ($V = Ah$), the impedance is

$$Z_{0V} = \frac{V^2}{P} = 2\omega\mu_0 hK \text{ ohms.} \tag{21}$$

In (20) and (21), the equations apply for a single side, as in Fig. 1. For the double-sided case (Fig. 2), these values should be divided by two.

A particularly interesting special case is that where the material is magnetized with a weak internal field, no greater than necessary for saturation. Assuming $H_i = 0$, the results are

$$\omega_0 = 0 \tag{22}$$

$$\mu = 1 \tag{23}$$

$$\frac{K}{\mu} = \frac{\omega_m}{\omega} \tag{24}$$

$$\beta_y = \omega\sqrt{\mu_0\epsilon_0\epsilon_f} \tag{25}$$

$$\alpha_x = \omega_m\sqrt{\mu_0\epsilon_0\epsilon_f} \tag{26}$$

$$Z_{0V} = 2\omega_m\mu_0 h. \tag{27}$$

Under these conditions and assumptions, this mode of propagation is predicted to be free of dispersion over all frequencies, to have a constant characteristic impedance, and to have a constant transverse decay rate α_x in the x direction. In practical cases, however, ferrite materials exhibit high losses at low internal fields at frequencies substantially lower than ω_m. The effects of fringing fields, neglected here, are more significant at high frequencies. For frequencies below ω_m, this appears

to be the only mode possible, but above ω_m, other modes of propagation can exist in the ferrite zone if the line is sufficiently wide. For these reasons, there are finite limits to the frequency band for utilization of this mode in practical devices.

Case 2: Finite-Width Lossless Lines

In the general case, each mode must include the two solutions with two arbitrary constants. A number of TE modes are possible in lines of sufficient width. We may distinguish these by an order n, where n is the number of E-field nulls found within zone I. The *dominant* mode, for which $n=0$, is the most important. In this approximation, which neglects fringing fields, x variations are exponential in the zero mode. In the higher order modes, sinusoidal x variations occur.

For the zero or dominant mode, the equations of case 1 apply. As $H_y=0$ everywhere, we need only consider the finite range of x from zero to a. The characteristic impedance, for a single ferrite slab, is given by

$$Z_{0I} = \frac{h\omega\mu_0 K}{2 \tanh (\alpha_x a/2)} . \tag{28}$$

Z_{0V} is an ambiguous concept in this geometry, but the other equations of Case 1 apply directly.

This approximate analysis which neglects fringing fields, indicates that the dominant mode is TEM in character with only E_z and H_x field components. Equation (25) indicates that it will propagate in frequency ranges where plane waves are cut off because μ_{eq} is negative. However, cut-off phenomena occur for frequencies near resonance ω_0, where μ is negative. In cases where the ferrite is magnetized with a low internal field H_i, propagation will be possible over very wide bands, although high losses are normally found at low frequencies, substantially below ω_m. Figs. 1 and 2 show the field configurations for this mode. The effect of the ferrite is to force the energy toward one side of the line. To the extent that fringing fields can be neglected, the degree of asymmetry is independent of frequency if the internal dc field is weak ($H_i \to 0$).

For the higher order modes, γ_x is imaginary and it is appropriate to use equations in which the x variations are sinusoidal. Equations (1)–(3) can be rewritten accordingly. Using new arbitrary constants C and D, the equations are

$$E_z = \{C \cos (\beta_x x) + D \sin (\beta_x x)\} e^{-j\beta_y y} \tag{29}$$

$$H_y = \frac{j}{\omega\mu_0\mu_{eq}} \left(\beta_x (C \sin (\beta_x x) - D \cos (\beta_x x)) - \beta_y \frac{K}{\mu} (C \cos (\beta_x x) + D \sin (\beta_x x)) \right) e^{-j\beta_y y} \tag{30}$$

$$H_x = \frac{1}{\omega\mu_0\mu_{eq}} \left(\frac{K}{\mu} \beta_x (-C \sin (\beta_x x) + D \cos (\beta_x x)) + \beta_y (C \cos (\beta_x x) + D \sin (\beta_x x)) \right) e^{-j\beta_y y}. \tag{31}$$

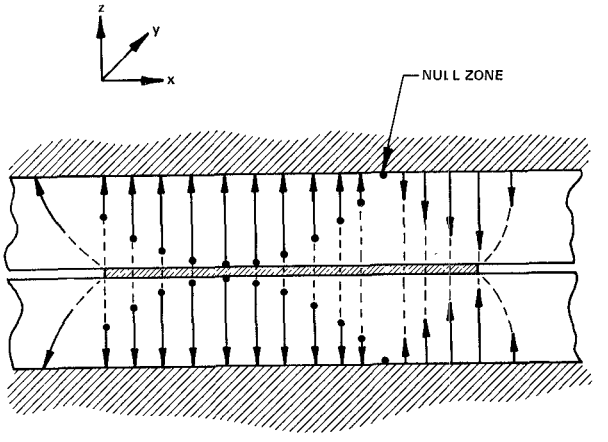

Fig. 3. E_z field configuration in first higher order mode. H_y nulls are found at edges; fields have sinusoidal variations with x.

Again, the boundary conditions are $H_y=0$ at $x=0$ and $x=a$. Using (30) we obtain

$$\beta_x D - \beta_y C \frac{K}{\mu} = 0 \tag{32}$$

$$\left(-\beta_x C - \beta_y \frac{K}{\mu} D\right) \sin (\beta_x a) + \left(\beta_x D - \beta_y \frac{K}{\mu} C\right) \cos (\beta_x a) = 0. \tag{33}$$

Solution of these equations requires that

$$\beta_x = \frac{n\pi}{a} \tag{34}$$

$$\beta_y = \sqrt{\omega^2\mu_0\epsilon_0\epsilon_f\mu_{eq} - (n\pi/a)^2} \tag{35}$$

$$\frac{D}{C} = \frac{K}{\mu} \sqrt{\frac{\omega^2\mu_0\epsilon_0\epsilon_f\mu_{eq}}{(n\pi/a)^2} - 1}. \tag{36}$$

The radicals must be internally positive in these solutions. For each such higher order wave of order n, a cut-off frequency may be determined by setting the radical equal to zero.

Fig. 3 shows a sketch of the fields for the first-order wave of this type. There is a single E-field null in the central region. H_y nulls occur at the edges. The pattern is asymmetrical with the null displaced from the axis. This class of mode cannot propagate for frequencies and magnetization conditions such that $\mu_{eq}<0$, even for very lines. In such cases, only the dominant or edge-guided mode can propagate.

IV. Edge Loading in Nonreciprocal Devices: Basic Principles and Equations

In lines of finite width, analyzed in Case 2, propagation occurs in both $\pm y$ directions with equal phase velocities and loss. However, the field patterns are laterally reversed, as mirror images, for the two directions of propagation. Similarly, the patterns may be reversed by reversing the sense of the magnetization. In the dominant mode, the energy will shift from one

TABLE I
PARAMETERS USED IN ISOLATOR COMPUTATION OF FIG. 4

$4\pi M = 1760$ G
$\epsilon_f = 16$
$H_i = 0$ $(\omega_0 = 0)$
$\omega_m/2\pi = 4.928$
$\mu = 1$
$a = 0.5$ cm
$\mu_{eq} = 1 - (\omega_m/\omega)^2$
$K = \omega_m/\omega$
$R_s = 150$ ohms/square

side to the other with a field reversal or wave direction reversal.

To obtain nonreciprocal behavior, the structure may be perturbed in an asymmetrical way. With resistive loading on one side only, high transmission loss will occur for the propagation direction for which the energy is concentrated on the lossy side, and lower loss for the oppositely directed wave where the energy is on the opposite side. This device is a new form of field-displacement isolator.

Nonreciprocal phase shift can be obtained by asymmetrical reactive loading of the opposite sides of the line, for example, by adding high-dielectric-constant material at one edge and using a low-dielectric-constant material at the other edge. When the energy is concentrated on the high-dielectric side, the wave will be slowed, giving greater phase shift; for the reverse wave, the energy will be greater at the low-dielectric side, giving reduced phase shift. By reversal of the magnetic field, the phase of transmission for a unidirectional wave will be equivalently changed.

Mode analysis, including edge-loading effects, can be accomplished using (1)–(9). At the two edge boundaries of zone I it is necessary to match the lateral wave admittance of the ferrite to that of the loaded edge. This is defined as the quotient H_y/E_z. For zone I this is the ratio of (2) to (1) at $x=0$ and $x=a$, which are matched to the wave admittances at the edges of zone II and III, respectively.

An accurate analysis must include the admittances of the fringing fields of the stripline or microstrip as well as that of any applied conductance or susceptance. In Section V first-order approximations are presented for the fringing-field admittances in the stripline or microstrip case. For the general equations hereafter it is assumed that zone II presents an unspecified edge admittance Y_{2x} in (ohms/square)$^{-1}$. Similarly for zone III, we have Y_{3x}. These admittances may be complex or imaginary and may be functions of the propagation constant γ_y as well as of frequency.

To simplify the equations and their solution, the following normalizing substitutions are used:

$$\beta_d = \omega\sqrt{\mu_0\epsilon_0\epsilon_f} \tag{37}$$

$$p_x = \gamma_x/\beta_d \tag{38}$$

$$p_y = \gamma_y/\beta_d \tag{39}$$

$$G_0 = \sqrt{\epsilon_0\epsilon_f/\mu_0}. \tag{40}$$

For the boundary at $x=0$, the following matching equation is obtained:

$$jp_x\left(1-\frac{B}{A}\right)-\frac{K}{\mu}p_y\left(1+\frac{B}{A}\right)=\frac{Y_{2x}}{G_0}\mu_{eq}\left(1+\frac{B}{A}\right). \tag{41}$$

For the boundary at $x=a$,

$$jp_x\left(1-\frac{B}{A}e^{2\beta_d p_x a}\right)-\frac{K}{\mu}p_y\left(1+\frac{B}{A}e^{2\beta_d p_x a}\right)+\frac{Y_{3x}}{G_0}\mu_{eq}\left(1+\frac{B}{A}e^{2\beta_d p_x a}\right)=0. \tag{42}$$

From (4) the normalized dispersion equation is

$$p_x = \sqrt{-p_y^2-\mu_{eq}} \tag{43}$$

which may be substituted into (41) and (42). This reduces the problem to two equations, with two unknowns p_y and B/A. If either Y_{2x} or Y_{3x} is resistive, or if losses in the ferrite are to be included, solution of these equations is tedious.

Case 3: Field-Displacement Isolator

A numerical solution has been carried out for a resistive wall case in which fringing fields were again neglected. At one wall, $x=0$, a resistive film is assumed to be shunting the line edge to the ground plane in the y–z plane. Thus it is assumed that

$$Y_{2x} = 1/R_s \tag{44}$$

$$Y_{3x} = 0 \tag{45}$$

where R_s is the resistance in ohms per square. The assumed parameters, neglecting ferrite losses, are given in Table I.

A digital computer was programmed in the following manner. A trial solution was chosen for p_y. This was substituted in (43), giving a value for p_x. Both were substituted into (41), which was then solved for B/A. These values were then substituted into (42), the left-hand side being treated as a function $F(p_y)$. A search routine was used which repetitively chose new values for p_y such as to reduce $F(p_y)$ to zero. The program allowed complex values of p_y, p_x, B/A, etc.

As expected, multiple solutions were found for both directions of propagation. These correspond to the various modes of propagation described under Case 2. If the initial choice for p_y was in the approximate vicinity of one of the solutions, the search routine quickly and automatically converged to the proper value. If the initial value was poorly chosen, the final value found by the machine was not always that for the mode desired at that point of the study. Solutions for the zero- and first-order modes in both directions were obtained in the frequency range of 3–15 GHz. The computed attenuations for these modes are plotted in Fig. 4.

The curves show a high ratio of forward-to-reverse transmission for the frequency range 3–10 GHz. Above 10 GHz we see that the first-order mode in reverse has

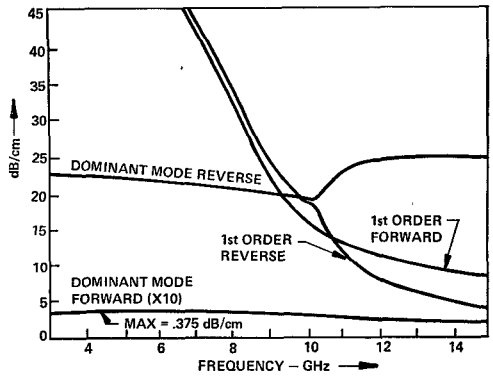

Fig. 4. Computations for stripline field-displacement isolator, giving loss in dB/cm for parameters of Table I. Fringing fields were neglected and a resistive film is assumed to be shunted between center conductor and ground planes on one side of zone I.

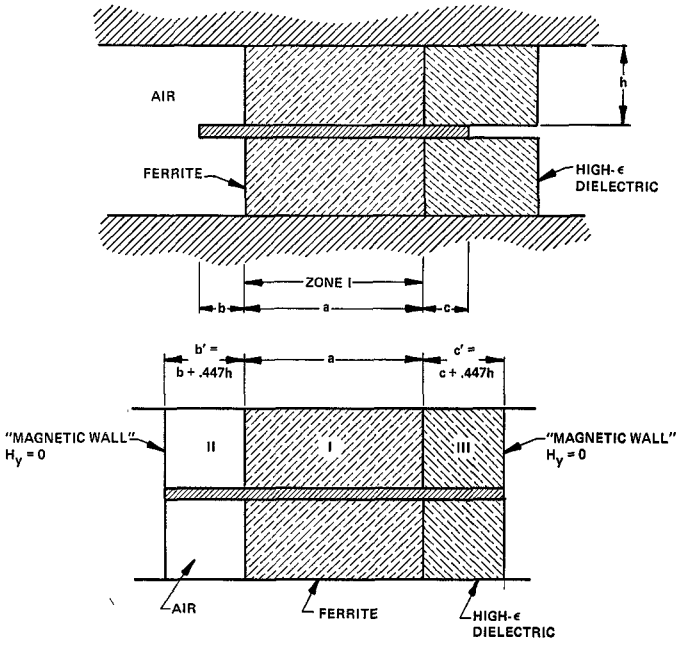

Fig. 5. Phase-shifter configuration and its approximate equivalent in analyzable form.

a rapidly decreasing attenuation, which can seriously degrade the isolation in a practical device.

Case 4: Nonreciprocal Phase-Shifter Analysis

One form of phase shifter can be constructed as illustrated in Fig. 5. This is a stripline version, but microstrip models are also possible. Here a relatively wide stripline is used, but three separate dielectric media are involved. The central zone is filled with ferrite, the left side of the conductor is terminated in a low-dielectric-constant region (such as air) and the right side in a high-dielectric-constant ceramic (such as Rutile).

The analysis should include some estimate of the effects of the fringing fields, as these are quite significant here. The approach is to modify the model into an analyzable geometry which is intuitively deduced to be approximately equivalent. The model chosen is illustrated in Fig. 5(b). Here a simple rectangular region is is divided into three zones, one air, one ferrite, and one ceramic. This includes vertical outer boundaries which are magnetic walls for which H_y/E_z must be zero. To include the effects of the fringing fields of the real model, zones II and III are widened by an amount which is estimated will include the excess capacitance and reduction of inductance associated with the fringing fields. Rectangular coordinates are used, and zones II and III are terminated at a magnetic wall. A nonmagnetic stripline of width W' between magnetic walls will have a characteristic impedance

$$Z_0 = \sqrt{\mu_0/\epsilon_0\epsilon_f}\, h/2W'.$$

Examination of published data [4] on the impedance of striplines indicates that this formula will be approximately correct for a stripline of width W if W' is increased over the real width W by the spacing $0.894h$, that is, if $W' \simeq W + 0.894h$. For this reason we presume that zone II in Fig. 5 should have a width $b' \simeq b + 0.447h$ and zone III should have a width $c' \simeq 0.447h$.

We wish to determine the edge admittances of zones II and III, to be matched to the edge admittance on either side of zone I. The field equations for these zones can be directly written, using any standard text on electromagnetic theory. For zone II, in air, we have slow-wave solutions, with hyperbolic functions for x variations. Here taking $x = 0$ at the magnetic wall,

$$\beta_0^2 = \omega^2\mu_0\epsilon_0 \tag{46}$$

$$E_z = A \cosh\left(\beta_0 x \sqrt{\frac{\beta_y^2}{\beta_0^2} - 1}\right) e^{-j\beta_y y} \tag{47}$$

$$H_y = jA \sqrt{\frac{\epsilon_0}{\mu_0}} \sqrt{\frac{\beta_y^2}{\beta_0^2} - 1} \cdot \sinh\left(\beta_0 x \sqrt{\frac{\beta_y^2}{\beta_0^2} - 1}\right) e^{-j\beta_y y} \tag{48}$$

$$Y_{2x} = \frac{H_y}{E_2} = j \sqrt{\frac{\epsilon_0}{\mu_0}} \sqrt{\frac{\beta_y^2}{\beta_0^2} - 1} \cdot \tanh\left(\beta_0 b' \sqrt{\frac{\beta_y^2}{\beta_0^2} - 1}\right). \tag{49}$$

For zone III, where the dielectric constant is ϵ_3, $\epsilon_2 > \epsilon_f$, the phase velocity will be faster than the velocity of light in that material. We require fast-wave solutions with sinusoidal x variations. Again, if $x = 0$ at the magnetic wall,

$$\beta_d^2 = \omega^2\mu_0\epsilon_0\epsilon_3 \tag{50}$$

$$E_z = A \cos\left(\beta_d x \sqrt{1 - \frac{\beta_y^2}{\beta_d^2}}\right) e^{-j\beta_y y} \tag{51}$$

$$H_y = -jA \sqrt{\frac{\epsilon_0\epsilon_3}{\mu_0}} \sqrt{1 - \frac{\beta_y^2}{\beta_d^2}} \cdot \sin\left(\beta_d x \sqrt{1 - \frac{\beta_y^2}{\beta_d^2}}\right) e^{-j\beta_y y} \tag{52}$$

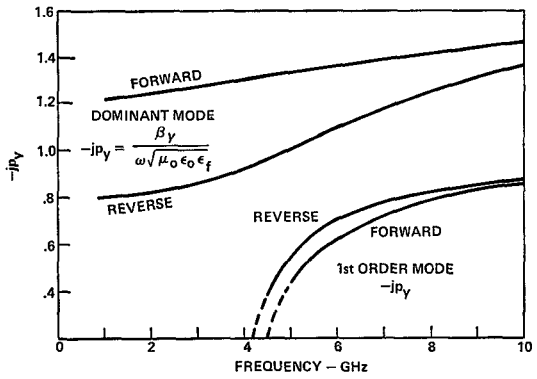

Fig. 6. Computations of normalized propagation constant for a nonreciprocal phase shifter of type shown in Fig. 5, using parameters of Table II.

TABLE II

ASSUMED PARAMETERS FOR PHASE-SHIFTER COMPUTATIONS OF FIG. 6

$4\pi M = \pm 690$ G
$H_i = 0$ ($\omega_0 \simeq 0$)
$a = 0.75$ cm
$\epsilon_f = 15$
$\epsilon_2 = 1$
$\epsilon_3 = 45$
$b' = 0.25$ cm
$c' = 0.1$ cm

$$Y_{3x} = \frac{H_y}{E_z} = j\sqrt{\frac{\epsilon_0\epsilon_3}{\mu_0}}\sqrt{1 - \frac{\beta_y^2}{\beta_d^2}} \cdot \tan\left(\beta_d c' \sqrt{1 - \frac{\beta_y^2}{\beta_d^2}}\right). \quad (53)$$

In the preceding, equations for the edge admittances have been given without regard to proper orientation with respect to the coordinates for our model of Fig. 5. Looking outward from zone I, the edge admittance of the air-filled zone will be inductive, and that of the dielectric-filled zone will be capacitive if the width c' is narrow.

Equations (41) and (42) are used to find the propagation constants γ_y and γ_x, using (49) and (53) for the edge admittances Y_{2x} and Y_{3x}. Using the same computer program as under Case 3, plots were obtained of the normalized propagation constant p_y for assumed lossless conditions, with the parameters given in Table II.

Plots of the normalized propagation constant p_y are given in Fig. 6. Here values are shown for the dominant mode and the first-order mode over the frequency range 1–10 GHz. The two values given are for the two directions of propagation assuming a constant magnetization, or alternately, are for the same wave direction, assuming that the magnetization has been reversed.

V. FRINGING-FIELD APPROXIMATIONS

A. Stripline Geometry

This section applies to devices as shown in Fig. 2, where the magnetized ferrite substrates are wide compared with the center conductor. The RF magnetic

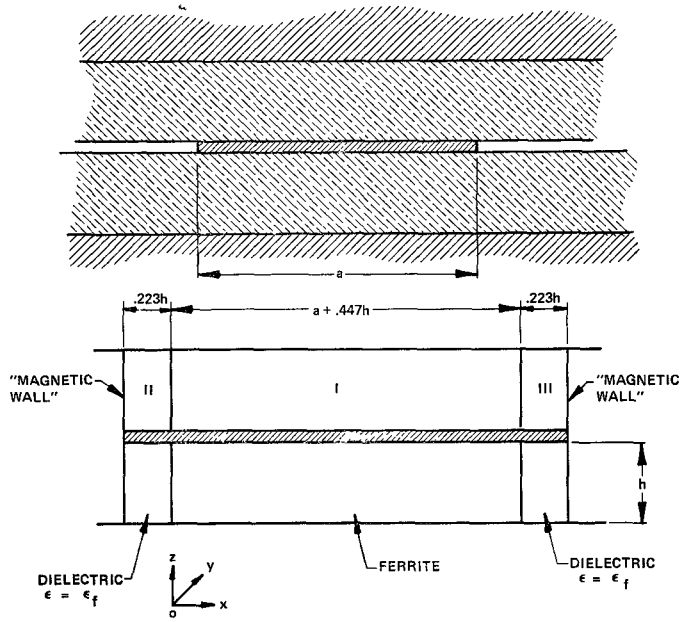

Fig. 7. Alternative geometry for analysis of stripline, including fringing-field correction.

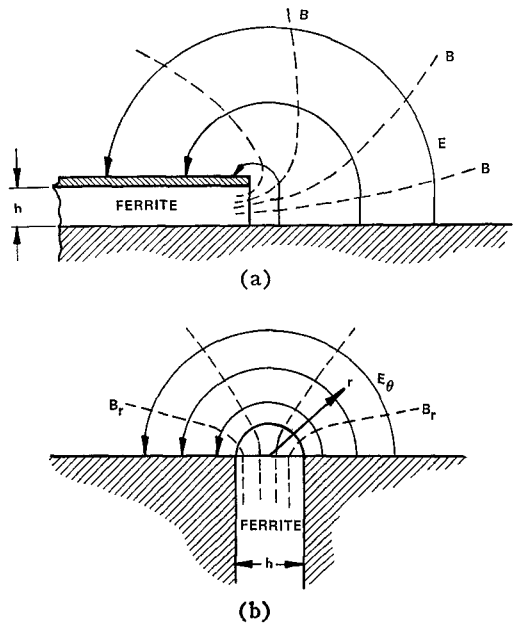

Fig. 8. Geometrical transformation for approximate analysis of microstrip fringing fields. Cylindrical coordinates outside are bridged onto rectangular coordinates for ferrite zone. (a) Edge of microstrip. (b) Approximate equivalent.

fields curve around the edges and form closed loops. However, these fields, in the dominant mode, are stronger at one side than the other. Where the H fields are vertical (in the z direction), parallel to the RF magnetization, the ferrite may be assumed to behave as a simple nonmagnetic dielectric, provided the ferrite is saturated.

The technique of analysis used is smaller to that for the phase shifter in Case 4. Again, the geometry is "deformed" into rectangular coordinates, with a magnetic wall at each extreme x boundary. The intuitive suggestion is to widen the line as before by an amount

of $0.447h$ on each side. Of the excess, it is assumed that one half behaves as fully magnetized ferrite and one half as nonmagnetic dielectric of the same dielectric constant. The modified geometry is pictured in Fig. 7. As in Case 4, it is suggested that zone I be widened by a total amount of $0.447h$, and zones II and III be of width $0.223h$, filled with dielectric of susceptability ϵ_f.

The analysis can proceed as in Case 4 and need not be repeated here. Study of the equations shows that the propagation constant of the dominant mode is affected little by the fringing fields, particularly if the internal field H_i is small. The characteristic impedance, however, may be significantly reduced by inclusion of these fringing fields.

B. Microstrip Geometry

Fringing fields are more significant in this geometry, particularly at the higher frequencies. The geometric transformation is illustrated in Fig. 8, where only one edge is analyzed. It is presumed that the upper conductor is approximately coplanar with the ground plane, and that the external electric fields are semicircular. The external zone is analyzed in cylindrical coordinates, and the small semicircular zone between the rectangular region and the cylindrical region is ignored. Our problem, as before, is to determine a value for the edge admittance H_y/E_z, using the cylindrical coordinates of Fig. 8.

In cylindrical coordinates θ, z, r, the appropriate TE mode is described by the field components E_θ, H_r, H_z as follows [5]:

$$H_z = Ae^{-j\beta_z z}H_0^{(1)}(jk_c r) \tag{54}$$

$$E_\theta = -\frac{A\omega\mu_0 e^{-j\beta_z z}}{k_c}H_1^{(1)}(jk_c r) \tag{55}$$

$$H_r = \frac{A\beta_z r^{-j\beta_z z}}{k_c}H_1^{(1)}(jk_c r) \tag{56}$$

$$k_c^2 = \beta_z^2 - \omega^2\mu_0\epsilon_0. \tag{57}$$

The preceding apply only if k_c^2 is positive as defined in (57).

A transverse wave admittance can be defined as

$$\left|\frac{H_z}{E_\theta}\right| = \left|\frac{k_c}{\omega\mu_0}\frac{H_0^{(1)}(jk_c r)}{H_1^{(1)}(jk_x r)}\right|. \tag{58}$$

The Hankel functions are tabulated by Jahnke and Emde [6]. The function $H_0^{(1)}$ is imaginary so that H_r and E_θ are in phase and H_z is in quadrature. The transverse wave admittance is also imaginary.

To match this admittance to the ferrite zone, we assume (with some error) that H_z above is equivalent to H_y in our rectangular coordinates at $x=0$. It is also assumed (with some error) that E_θ will be $2/\pi$ times E_z in the rectangular coordinates at $x=0$. Thus for the admittance match, we ignore the small semicylindrical zone of the external cylindrical coordinate system within the radius $h/2$. The appropriate matching admittance

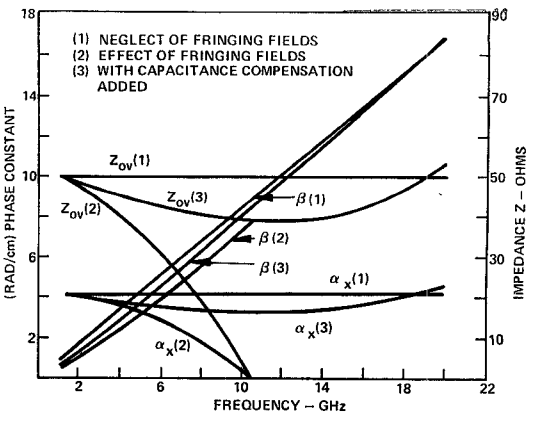

Fig. 9. Computations of edge-guided mode parameters for a semi-infinite-width microstrip line, using data of Table III. Ideal characteristics of first case are severely affected by fringing fields at high frequency in second case. Significant compensation is obtainable by capacitive loading of propagating edge (third case).

TABLE III
PARAMETERS FOR COMPUTATIONS OF FIG. 9

$4\pi M_s = 1780$ G (saturated)
$\epsilon_f = 16$
$h = 0.025$ in
$H_i = 0$
Compensating edge capacitance = 1.25 pF/cm

Y_{2x} is, therefore, estimated to be

$$Y_{2x} = \frac{k_c\pi}{2\omega\mu_0}\frac{H_0^{(1)}(jk_c h/2)}{H_1^{(1)}(jk_c h/2)}. \tag{59}$$

The character of the preceding is such that the admittance looking outward is imaginary and inductive. The phase velocity will be increased by the effects of fringing fields.

It should be recognized that the above approximation is somewhat inaccurate, and is believed to be too large in magnitude. We have not included the effects of the dielectric material outside the edge of the microstrip in this transformation.

Approximate computations have been made using this formulation for the edge-guided mode in an infinitely wide microstrip. The assumed parameters are given in Table III.

These results are given in Fig. 9. Three cases are shown. One represents the solutions of Case 1 neglecting fringing fields. Another shows the effects of fringing fields according to the preceding equations, and a third includes an addition of capacitive susceptance to the edge to compensate for the inductive susceptance of the fringing fields. The effect of the fringing field correction above is quite severe at the higher frequencies, causing a disappearance of this mode at about 10.5 GHz. Above this frequency the transverse decay constant α_x has vanished and solution of the wave equations requires sinusoidal x variations. By the addition of a small capacitive perturbation to the edge, however, this effect can be partially compensated, as the curves show.

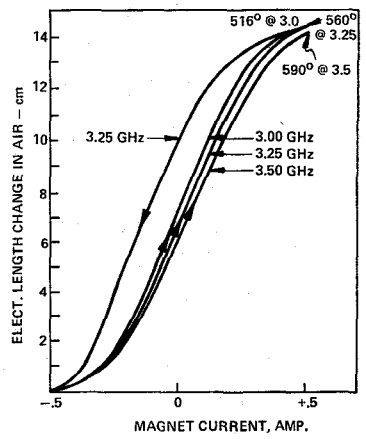

Fig. 10. Data obtained with experimental phase shifter described. Over this frequency range, change in electrical length is plotted as magnetic field is varied. Hysteresis effect is largely caused by steel magnetic structure used.

It will be noted that no model and no analysis has been made for the narrow microstrip line. This is a more difficult problem, deserving of further study. For this case the fringing fields tend to dominante the characteristics and can no longer be considered as perturbations. Furthermore, the fringing fields of the two sides overlap, and are directly coupled in the region above the conductor. Such lines have been used successfully and repeatedly in various devices, including phase shifters [8], circulators, and tunnel diode amplifiers [9]. Measurements of phase-shift data are given by Buck [10], and an analysis of the coupled-line problem is given by Weiss [11].

VI. Experimental Results

We report here some experiments with phase shifter and isolator devices which resemble the models analyzed but are not exact equivalents. The data are not intended to show quantitative agreement with the theory.

A phase shifter was constructed in stripline form using Trans-Tech GL610 material with $4\pi M_s = 680$ G and a dielectric constant of 14.5. Two ferrite slabs of 4.5 by 0.300 by 0.100 in were used. As in Fig. 5, the center conductor extended into air on one side and ceramic dielectric on the other side. Steel plates were used as ground planes, and a magnetic coil was added for field control. The coil contained 80 turns. Step-type impedance transformers were used for approximate matching to 50-Ω lines.

Fig. 10 shows data of phase shift versus coil current for three different frequencies, always starting at negative values of current. One case also shows the returning characteristic, illustrating the effect of magnetic hysteresis in the materials used. We have plotted the change in electrical length rather than angles. This is the length change of an air-filled trombone coaxial line, used to maintain balance in the phase bridge used.

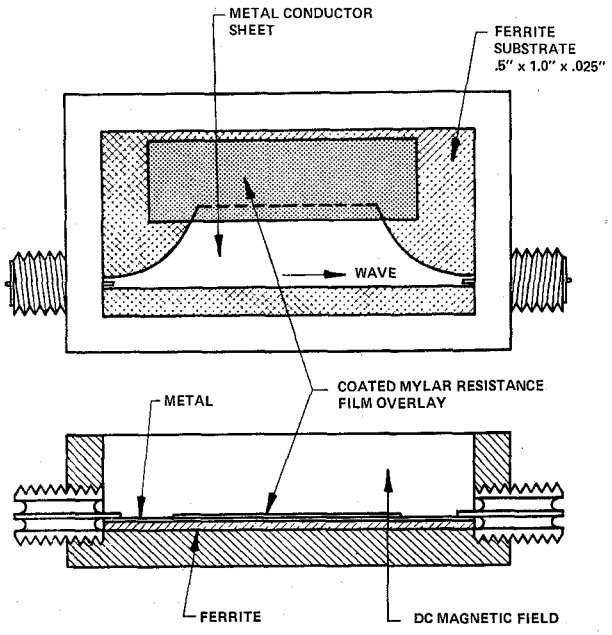

Fig. 11. Experimental microstrip isolator, giving performance data of Fig. 12.

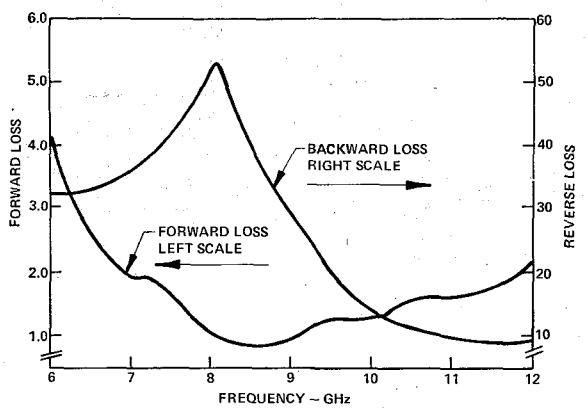

Fig. 12. Measured forward and reverse loss characteristics of isolator similar to Fig. 11.

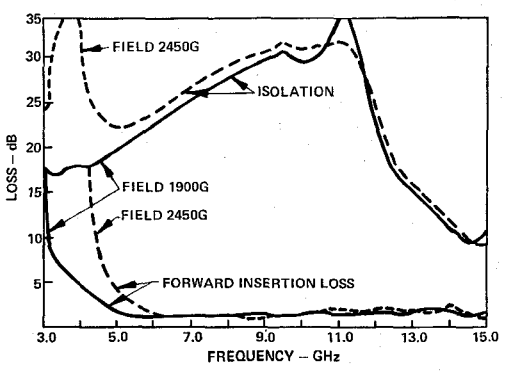

Fig. 13. Measured forward and reverse loss characteristics of isolator similar to Fig. 11, with added capacitive compensation along low-loss edge.

It will be noted that the length change is nearly constant with frequency, indicating a phase change roughly proportional to frequency. The curves of Fig. 6 also show this character in the frequency range 3–3.5 GHz. In this band we obtained about 1.5 full cycles of phase shift. Attenuation averaged 0.8 dB.

A microstrip isolator was constructed as shown in Fig. 11. Here the wide microstrip line was approximately matched to the input and output 50-Ω lines by curved tapers. Loss was applied to one edge by overlaying a Mylar film coated with thin-film metallization. Data as shown in Fig. 12 were obtained with this device.

Based upon our theory of fringing-field degradation of the edge-guided mode, we then applied capacitance loading to the long straight edge of the conductor. This device gave isolator effects over a much wider band as shown in Fig. 13.

These devices used Trans-Tech ferrite material type G113, 0.025 in thick. The device was 1 in long. The fields shown in Fig. 13 were measured external to the ferrite. Internal fields are reduced by the saturation magnetization, ($H_i \simeq H_{ext} - 4\pi M_s$ if $H_{ext} > 4\pi M_s$). This material has a saturation magnetization of 1780 G and a dielectric constant of 15.

VII. Conclusions

We have presented a theory for the propagation modes in wide ferrite stripline and microstrip devices, including the effects of fringing fields by approximation techniques. Physical descriptions of the wave patterns have been given. The dominant mode normally exhibits a reversible field-displacement effect with energy concentrated along one side of the line.

We have also described a new form of isolator and a new phase shifter which use the field-displacement effect of the dominant mode. Experimental data have been given which illustrate the usefulness of these devices.

Acknowledgment

Significant technical contributions were made by L. C. Nelson, P. Setzco, L. Kou, and C. Delise.

References

[1] B. Lax and K. J. Button, *Microwave Ferrites and Ferrimagnetics*. New York: McGraw-Hill, 1962.
[2] P. J. B. Clarricoats, *Microwave Ferrites*. New York: Wiley, 1961, pp. 113–116.
[3] R. F. Soohoo, *Theory and Applications of Ferrites*. Englewood Cliffs, N. J.: Prentice-Hall, 1960, pp. 132–137.
[4] S. B. Cohn, "Shielded coupled-strip transmission lines," *IRE Trans. Microwave Theory Tech.*, vol. MTT-3, Oct. 1955, pp. 29–38.
[5] S. Ramo and J. R. Whinnery, *Fields and Waves in Modern Radio*, 2nd ed. New York: Wiley, 1953, pp. 357–358.
[6] E. Jahnke and F. Emde, *Table of Functions*, 4th ed. New York: Dover, 1945, pp. 236–243.
[7] M. E. Hines, "A new microstrip isolator and its application to distributed diode amplification," in *1970 IEEE Int. Microwave Symp. Dig.*, pp. 304–307.
[8] G. T. Roome and H. A. Hair, "Thin ferrite devices for microwave integrated circuits," *IEEE Trans. Microwave Theory Tech.*, vol. MTT-16, July 1968, pp. 411–420.
[9] J. D. Welch, "Beam-lead tunnel diode amplifiers on microstrip," in *1970 IEEE Int. Microwave Symp. Dig.*, p. 212 (IEEE Cat. No. 70-C-10MTT).
[10] D. C. Buck, "Ferrite microstrip propagation," in *1970 IEEE Int. Microwave Symp. Dig.*, p. 117 (IEEE Cat. No. 71-C-66).
[11] J. A. Weiss, "An analysis of nonreciprocal microstrip," in *1970 IEEE Int. Microwave Symp. Dig.*, p. 404 (IEEE Cat. No. 70-C-10MTT).
[12] M. E. Biodwin, "Propagation in ferrite-filled microstrip," *IRE Trans. Microwave Theory Tech.*, vol. MTT-6, Apr. 1958, pp. 150–155.

On the Design of Optimum Dual-Series Feed Networks

WILLIAM R. JONES, SENIOR MEMBER, IEEE, AND EDWARD C. DuFORT, MEMBER, IEEE

Abstract—**A computer-implemented procedure is presented for the design of optimally efficient dual-series feed networks for use in waveguide phased arrays where the network directional couplers are limited in their values of maximum coupling by geometrical and bandwidth requirements. The theory of the design procedure is outlined and results for the design of sum and difference pattern element excitations for typical coupler limitations are presented.**

Manuscript received August 12, 1970; revised November 12, 1970.
The authors are with the Ground Systems Group, Hughes Aircraft Company, Fullerton, Calif. 92634.

Introduction

A SIGNIFICANT problem in the design of monopulse array antennas is to derive line source microwave feed networks which yield two desired array excitations with optimum efficiency and which are compatible with the geometrical constraints imposed upon them for use in two-dimensional arrays. This latter factor places significant limitations on the feed networks with respect to the types of directional